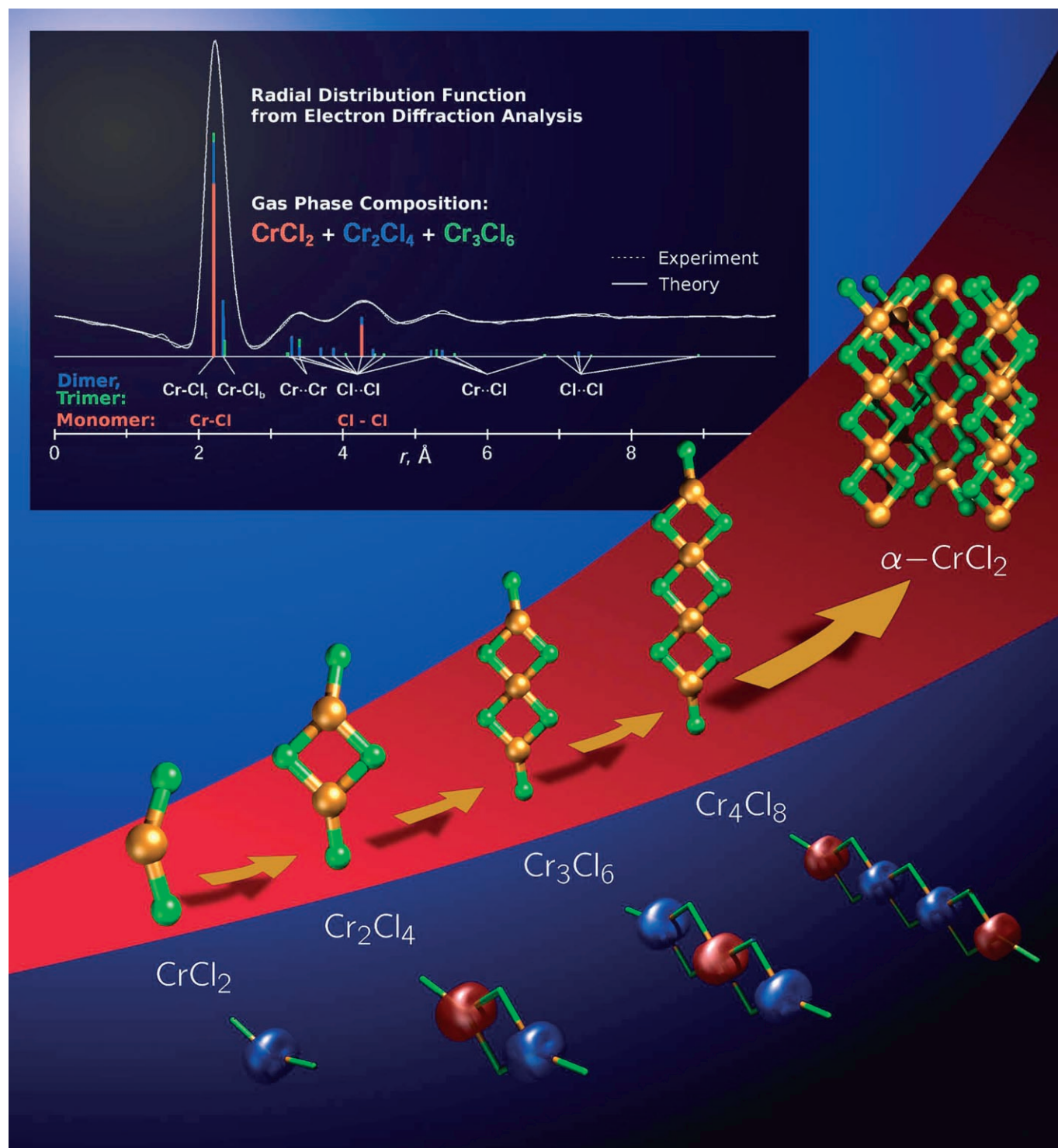


# The Elusive Structure of $\text{CrCl}_2$ —A Combined Computational and Gas-Phase Electron-Diffraction Study

Brian Vest,<sup>[a]</sup> Zoltán Varga,<sup>[b]</sup> Magdolna Hargittai,<sup>\*[b]</sup> Andreas Hermann,<sup>[a]</sup> and Peter Schwerdtfeger<sup>\*[a]</sup>



**Abstract:** Chromium dichloride poses a challenge to the structural chemist. Its different forms of aggregation and association display all well-known structural distortions induced by vibronic interactions. The monomeric molecule has a Renner–Teller distorted bent geometry, the crystal exhibits strong Jahn–Teller distortion, and the oligomers have slightly distorted four-membered-ring structures due to the pseudo-Jahn–Teller effect. In this paper we report on the low-energy structures of the monomer and its clusters,  $\text{Cr}_2\text{Cl}_4$ ,  $\text{Cr}_3\text{Cl}_6$ , and  $\text{Cr}_4\text{Cl}_8$ , from unrestricted Kohn–Sham (broken-symmetry) density functional calculations.  $\text{CrCl}_2$  was also investigated at higher level, including coupled-cluster and state-average CASSCF computations. The global minima of the gas-phase clusters con-

sist of two-dimensional, antiferromagnetically coupled chains of  $\text{CrCl}_2$  units forming four-membered, doubly bridged  $\text{Cr}_2\text{Cl}_2$  rings, closely resembling the solid-state structure of  $\alpha\text{-CrCl}_2$ . Each Cr atom in these chains has spin quantum number  $S=2$ . This suggests that the  $\text{CrCl}_2$  nucleation starts very early on the structural chain motif found in the solid. There is only a very small change in energy from the antiferromagnetically to the ferromagnetically coupled Cr atoms, which indicates little spin-coupling between the metal cen-

ters. There is an approximately constant change in energy, about  $50 \text{ kcal mol}^{-1}$ , with every new  $\text{CrCl}_2$  unit during cluster formation. Information about the structure of these clusters was used in the re-analysis of high-temperature electron-diffraction data. The vapor at 1170 K contained about 77% monomeric molecules, 19% dimers, and a small amount of trimers. Monomeric  $\text{CrCl}_2$  was found to be bent with a bond angle of  $149(10)^\circ$ , in good agreement with our computations, which resulted in a Renner–Teller distortion of the lowest-energy  ${}^5\Pi_g$  electronic state into the bent  ${}^5B_2$  ground state. The vibrational spectrum of chromium dichloride is discussed and the thermodynamics of cluster formation from 1000–2000 K is examined.

**Keywords:** chromium dichloride • density functional calculations • electron diffraction • nucleation • Renner–Teller effect • structure elucidation

## Introduction


The electronic and structural properties of the seemingly simple first-row transition-metal dihalides have been debated by both theoreticians and experimentalists for many years.<sup>[1,2]</sup> Infrared (IR) spectroscopy and electron diffraction (ED) have been the primary means of determining the geometry of these systems. The ED study of  $\text{CrCl}_2$ <sup>[3]</sup> and  $\text{CrF}_2$ ,<sup>[4]</sup> and the IR spectroscopic studies of different chromium dihalides<sup>[5–12]</sup> have been reported previously. However, the unambiguous determination of their structure has been a problematic issue. According to mass spectrometric studies of chromium dihalides<sup>[13,14]</sup> their vapor phase is complex, as considerable amount of small clusters (up to tetramers) are

present beside the monomers. This fact makes the analysis of both electron diffraction and gas-phase spectroscopic results rather difficult, since the information concerning the monomeric molecules is buried among the ones corresponding to the different oligomers. Another difficulty for gas-phase spectroscopy is that chromium dihalides are rather involatile compounds and the high temperatures needed to vaporize their molecules complicate the interpretation of the IR spectra, because of significant occupation of excited vibrational and rotational levels. Furthermore, these molecules have low-energy bending modes that are often outside the range of spectrometers. IR spectroscopy is also insensitive to isotopic shifts of the asymmetric stretching mode for quasi-linear molecules with bond angles between  $150^\circ$  to  $180^\circ$ , and this makes the determination of their shape ambiguous.<sup>[15]</sup> Matrix-isolation infrared spectroscopic studies (MI-IR) might be a remedy to this problem, but they suffer from possible effects due to the interaction with the matrix.

The general agreement from the above-mentioned IR spectroscopic studies is that the structure of  $\text{CrCl}_2$  appears to be linear, with the primary evidence of linearity being the lack of a peak corresponding to the symmetric stretching frequency. However, due to its weak intensity, the symmetric stretching vibration for a quasi-linear molecule would be quite difficult to detect in the IR spectrum, and the possibility of non-linearity cannot be discarded. Further evidence for a possible bent structure stems from the earliest argon MI-IR experiment,<sup>[5]</sup> from which the authors reported that the frequency pattern for the asymmetric stretching mode closely resembled that of a molecule with a bond angle between  $120^\circ$  and  $150^\circ$ . The earlier ED experiment by one of us<sup>[3]</sup> reported a highly bent structure with a Cl–Cr–Cl bond

[a] B. Vest, A. Hermann, Prof. Dr. P. Schwerdtfeger  
Centre of Theoretical Chemistry and Physics (CTCP)  
The New Zealand Institute for Advanced Study  
Massey University (Auckland Campus)  
Private Bag 102904, North Shore MSC  
0745 Auckland (New Zealand)  
Fax: (+64)9-443-9779  
E-mail: p.a.schwerdtfeger@massey.ac.nz

[b] Z. Varga, Prof. Dr. M. Hargittai  
The Materials Structure and  
Modeling Research Group of the Hungarian Academy of Sciences  
Budapest University of Technology and Economics  
P.O.Box 91, 1521 Budapest (Hungary)  
Fax: (+36)1-463-4052  
E-mail: hargittaim@mail.bme.hu

 Supporting information for this article is available on the WWW under <http://www.chemistry.org> or from the authors. It contains experimental electron diffraction molecular intensities at two different camera ranges (Table S1) and Cartesian coordinates and energies (Table S2) of different cluster structures.

angle of 110°. However, later it was communicated that due to the more complicated vapor composition than assumed in the study, the result should be disregarded.<sup>[2]</sup> One of the aims of the present study is the re-analysis of the ED experiment with the help of information from our high-level computations of all species.

Quantum-chemical studies have become a powerful technique in aiding the interpretation of experimental data for CrCl<sub>2</sub>. Earlier ligand-field theory (LFT) was the accepted model to aid the interpretation of the spectra of transition-metal halides. LFT predicts that the transition-metal dihalides (MX<sub>2</sub>) would be linear in the gas-phase, with a high-spin metal center, and only ionic interactions between the metal and the halides. In a linear MX<sub>2</sub> molecule (*D*<sub>∞h</sub>-symmetry ligand field), the relative energies of the metal d orbitals are in the order of  $\delta_g < \pi_g < \sigma_g$ .<sup>[16,17]</sup> Hence, LFT together with Hund's rule predicts that CrCl<sub>2</sub> would have an electronic ground state of <sup>5</sup>Σ<sub>g</sub><sup>+</sup> with an open-shell electron configuration of  $\delta_g^2 \pi_g^2$ . The two earliest ab-initio calculations<sup>[18,19]</sup> agreed with this prediction, and the ground state of CrCl<sub>2</sub> was calculated to be the <sup>5</sup>Σ<sub>g</sub><sup>+</sup> state with the <sup>5</sup>Π<sub>g</sub> ( $\delta_g^2 \pi_g^1 \sigma_g^1$ ) and <sup>5</sup>Δ<sub>g</sub> ( $\delta_g^1 \pi_g^2 \sigma_g^1$ ) states being the first and second excited electronic states, respectively. However, the more recent density functional theory (DFT) calculations by Wang and Schwarz<sup>[20]</sup> and also by Bridgeman and Bridgeman<sup>[21]</sup> gave the energy sequence <sup>5</sup>Π<sub>g</sub> < <sup>5</sup>Σ<sub>g</sub><sup>+</sup> < <sup>5</sup>Δ<sub>g</sub>. Bridgeman also suggested, for the first time, that the first members of the transition-metal dihalide series might have a bent equilibrium geometry with a flat bending potential. At about the same time, Jensen<sup>[22]</sup> also determined a <sup>5</sup>B<sub>2</sub> ground state as a result of the Renner–Teller type bending of the <sup>5</sup>Π<sub>g</sub> state. He, again, noted a very flat bending potential with a barrier to inversion of only 100 cm<sup>-1</sup> at a bond angle of 144.3°. In a more recent paper, Nielsen and Allendorf<sup>[23]</sup> also predicted the <sup>5</sup>B<sub>2</sub> state as the ground state using coupled cluster theory, CCSD(T). They also reported that the <sup>5</sup>B<sub>2</sub> state was only 0.1 kcalmol<sup>-1</sup> lower in energy than the <sup>5</sup>Π<sub>g</sub> transition state, and this rather small energy difference is below the zero-point vibrational energy for the bending mode. Such a small energy difference makes the correct prediction of the ground-state symmetry a formidable task, and to this date a definite assignment of the electronic ground state of CrCl<sub>2</sub> remains an irresolute issue.

The breakdown of LFT for transition-metal dihalides was discussed extensively by Wang and Schwarz<sup>[20]</sup> and Bridgeman and Bridgeman.<sup>[21]</sup> The computations show that ligand-induced 3d–4s hybridization from the partially filled 3d subshell on Cr lowers the energy of the  $\sigma_g$  orbital and the strong  $\pi$ -donating properties of the halide ligands tend to increase the energy of the  $\pi_g$  orbital. Jensen showed that inclusion of electron correlation is also important in determining the correct electronic ground state of CrCl<sub>2</sub>; it increased the energy of the <sup>5</sup>Σ<sub>g</sub><sup>+</sup> and <sup>5</sup>Δ<sub>g</sub> states relative to the <sup>5</sup>Π<sub>g</sub> state by 3500 and 2600 cm<sup>-1</sup>, respectively. Apparently, scalar relativistic effects contributed less than 600 cm<sup>-1</sup>.<sup>[22]</sup>

The computations up until now focused on monomeric chromium dichloride. However, as discussed above, the

vapor phase of the chromium dihalides contains a large amount of oligomers as well. The only computation on such species was done on Cr<sub>2</sub>I<sub>4</sub>.<sup>[24]</sup> In this study, the structure was optimized with C<sub>2v</sub> symmetry and a high-spin (nonet) state was assumed to be the ground state. No other possible geometry or spin-state was investigated, neither were the trimeric and tetrameric species.

Computations of transition-metal dihalides face a number of serious difficulties. For transition-metal-containing compounds, wave-function-based methods are computer time intensive and often require a multireference treatment.<sup>[25]</sup> On the other hand, less costly DFT calculations are plagued with correctly describing strong correlation and multireference character in such systems.<sup>[26,27]</sup> As an example, Mott insulators of transition-metal compounds are not well described by the generalized gradient approximation (GGA) in DFT,<sup>[28]</sup> and one is forced to add an on-site Hubbard-like repulsion term (LDA+U approach<sup>[29]</sup>). Spin-symmetry breaking in transition-metal compounds and consequently spin–spin coupling in magnetic materials are also affected by these deficiencies.<sup>[30,31]</sup>

In this work, our goal was to determine the ground-state geometry of CrCl<sub>2</sub> species from the monomers to the tetramers, the infinite chain and the solid, at specific levels of theory and compare the low-lying isomers of different spin states. We also predict harmonic vibrational frequencies that are used to calculate the thermodynamics of the cluster formation within the temperature range used in the ED experiment. Finally, we carried out a reanalysis of the earlier ED experiment,<sup>[3]</sup> taking into consideration all possible species that can be present in the vapor at the experimental conditions.

## Experimental Section

**Computational methods:** To determine all possible low-energy structures for the CrCl<sub>2</sub> clusters, we performed geometry optimizations using unrestricted Kohn–Sham (UKS) density functional theory, which breaks spin-symmetry in these clusters (BS-DFT). As a starting point, we used the PW91 gradient-corrected exchange–correlation functional by Perdew et al.<sup>[32]</sup> with the Los-Alamos pseudopotentials and corresponding valence double-zeta basis sets (LanL2DZ) for Cr and Cl.<sup>[33,34]</sup> These preliminary calculations were carried out for a large variety of possible three-dimensional structures with chromium in different coordination and spin states. All minima that yielded energies within a window of 1 eV from the global minimum were considered for further refinement, except for the tetramer for which we chose a window of 0.5 eV because of the high computational costs. Using these geometries as a starting point, we carried out geometry optimizations using Becke's three-parameter hybrid functional (B3LYP),<sup>[35–38]</sup> which contains exact exchange and is known to give better geometries. Here we used a modified energy-consistent Stuttgart scalar relativistic small-core pseudopotential and corresponding valence basis set with a [8s8p7d3f]/(7s7p5d3f) contraction scheme for Cr.<sup>[39]</sup> An aug-cc-pVDZ basis set was used for Cl;<sup>[40]</sup> thus a total of 128 contracted basis functions were used for the monomer. To ascertain the effects of a larger basis set and different methods on the various low-energy oligomers, B3PW91<sup>[32,35]</sup> optimizations with a cc-pVTZ basis set for Cl<sup>[40]</sup> were also performed,<sup>[41]</sup> which is also known to perform well for metal halides.<sup>[42–44]</sup>

The singlet states of the  $\text{CrCl}_2$  clusters are symmetry broken in the single determinant description. If the closed-shell restricted Hartree–Fock approximation is applied, the configuration does not even resemble the singlet ground state. As a result, we found that the dimeric  $\text{Cr}_2\text{Cl}_4$  dissociates into two monomer subunits during the optimization at HF and MP2 levels of theory, and DFT leads to unreasonable geometries as well. For example, the restricted B3LYP calculation for  $\text{Cr}_2\text{Cl}_4$  gives an energy of 6.4 eV above the BS-DFT approach. Hence, a single-reference description is not sufficient anymore. Because of the open-shell nature of the  $\text{CrCl}_2$  electronic structure, we also performed complete active space self-consistent field calculations (CASSCF), followed by second-order perturbation theory (CASPT2) for both the monomeric and dimeric species, as well as coupled cluster calculations (CCSD(T)) for the monomer within a full active valence space. For the CASSCF calculations, initial guesses of the wavefunctions were obtained from restricted open-shell Hartree–Fock calculations. For the low lying  $^3\text{B}_2$ ,  $^5\Sigma_g^+$ ,  $^5\Pi_g$ , and  $^5\Delta_g$  states of the monomer, we applied CASSCF(16,15), which denotes 16 electrons distributed over 15 orbitals. This active space consisted of the five 3d metal orbitals on Cr ( $\delta_g$ ,  $\pi_g$ ,  $\sigma_g$ ) along with the 3p orbitals from both Cl. Also included in the active space were the virtual 4s and 4p orbitals on Cr. The geometry was kept at the optimized B3LYP distance, since an optimization was computationally not feasible. For the CASPT2 calculation, we had to reduce the active space to (4,5) for the  $^3\text{B}_2$ ,  $^5\Sigma_g^+$ ,  $^5\Pi_g$ ,  $^5\Delta_g$ ,  $^3\Sigma_g^-$ , and  $^1\Sigma_g^+$  states, which distributes four electrons in the metal 3d orbitals. Here we were able to carry out a geometry optimization. For the dimers, we used the same active space as for the monomers, which results in a CASSCF-(8,10) of the ten 3d metal orbitals on the Cr atoms. Only the singlet and nonet states of the dimer were examined, as these calculations became again prohibitively expensive, and the geometry was also fixed to that obtained from the B3LYP calculations. For the  $^5\Pi_g$  and  $^5\Delta_g$  states, a state-averaged CASSCF calculation had to be performed to correctly describe the multireference character in these states. All multireference calculations were performed using the program system Molpro.<sup>[45]</sup>

Harmonic vibrational frequencies were computed by standard analytical gradient techniques, which gave the zero-point vibrational energy correction, the enthalpy and the Gibbs free energies of atomization for a temperature range of 1000–2000 K and a pressure of 1 atm. Basis-set superposition errors (BSSE) for the clusters were calculated using the counterpoise correction by Boys and Bernardi,<sup>[46,47]</sup> but including two-body terms only.

To calculate the antiferromagnetically coupled infinite chain of  $\text{CrCl}_2$  we performed DFT calculations with the PW91 functional employing the projector augmented wave (PAW) method<sup>[48,49]</sup> with a plane wave basis set as implemented in the Vienna Ab-initio Simulation Package.<sup>[50]</sup> Using a supercell approach, neighboring chains were separated by at least 25 Å. Along the chain direction, two irreducible  $k$ -points were found sufficient to sample the Brillouin zone. Further details of these and the bulk crystal calculations can be found in reference [31].

**Electron diffraction analysis:** We decided to reanalyze the earlier electron diffraction experimental data by one of us (M.H.),<sup>[3]</sup> because of the possibility that larger species might have been present in the vapor beside the monomers and dimers that were taken into account in the original analysis.<sup>[2]</sup> The details of the experiment are given in reference [3], and the temperature of the experiment was  $1170 \pm 50$  K. Since the publication of the original article, a new set of electron scattering factors was published; these were used for the new analysis.<sup>[51]</sup> The experimental and theoretical molecular intensity and radial distribution curves are given in Figures 1 and 2; the experimental molecular intensities are given in Table S1 as supporting information. The first and largest peak on the radial distribution contains all Cr–Cl bond lengths, that is, those of the monomer and of the different clusters that were present in the vapor. According to the computation, there were three different bond lengths in the dimer and four different bond lengths in the trimer. This means altogether seven additional different Cr–Cl distances besides the monomer. It is clear that without some prior information about them, they could not be separately determined. Similarly, we needed information from other sources about the symmetry and structure of the oligomers present

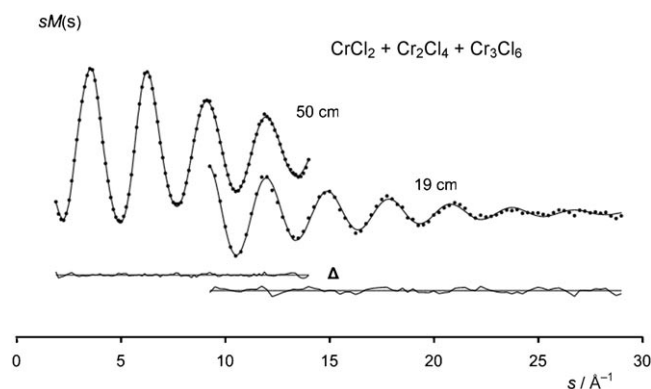


Figure 1. Experimental (dots) and calculated (solid line) electron diffraction molecular intensities and their differences ( $\Delta$ ) at two different camera ranges for a vapor composition of 77(4)% monomers, 19(4)% dimers, and 4(3)% trimers of chromium dichloride.

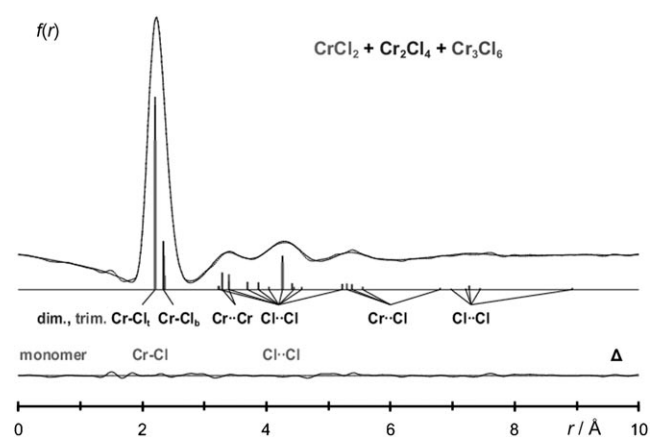


Figure 2. Experimental (dotted line) and calculated (solid line) radial distributions and their differences ( $\Delta$ ) corresponding to the molecular intensities of Figure 1. The contributions of different distances are indicated.

in the vapor in order to aid the electron diffraction analysis by way of applying them as constraints.

Our strategy was the following: we accepted as constraints, at least at the initial stages of the refinement, all the differences of the different cluster bond lengths from that of the monomer. It is known that the physical meaning of bond lengths coming from different techniques is different,<sup>[52]</sup> and simply taking over bond lengths from the computation (equilibrium bond length) to the analysis of electron diffraction data (from which we determine thermal average bond lengths) would be erroneous. However, taking the *differences* of bond lengths approximately cancels the difference between their physical meaning, and therefore, their use as constraints is an accepted procedure. The stretching vibrations of metal halides are usually anharmonic, and this influences the molecular intensities. The so-called asymmetry parameter ( $\kappa$ ), describing the stretching anharmonicity, can usually be refined. However, with so many closely spaced bond lengths this was impossible; therefore, we assumed the asymmetry parameter based on our experience with other transition-metal dihalides.<sup>[53]</sup>

Furthermore, we also accepted the bond angles of the dimer and trimer from the computation. We also carried out normal coordinate analyses using the program ASYM<sup>[54]</sup> based on the computed frequencies and force fields of all three species, in order to calculate vibrational amplitudes. These were used as starting parameters, and many of them were later refined during the analysis. The parameters that were refined at the

first stages of the analysis were the bond length and the vibrational amplitudes of the monomer molecule, the vapor composition, and the vibrational amplitudes of the other chromium–chlorine bond lengths grouped together with the monomer amplitude. We also refined the amplitudes of the most important nonbonded distances of the different species. The analysis was performed with the so-called static analysis, meaning that a thermally averaged structure was refined. Such a structure suffers from the shrinkage effect and usually has a lower symmetry than the equilibrium structure. Therefore, we introduced and refined the parameters describing the puckering motions of the dimers and trimers.

We found that with the above constraints, the agreement between the experimental and theoretical distributions was not satisfactory, especially in the region of the bond length, indicating that the constrained bond-length differences did not quite correspond to the measured structures. Therefore, we tried to carefully refine them, and they usually refined to somewhat smaller values than the computed ones. Since the computed bond-length differences were not exactly the same from different levels of computations, we decided that refinement of these values was justified. Further, we let the bond angle of the monomer and those of the dimer also refine. They stayed close to the computed values.

Looking at the radial distribution curve, it can be seen that most of the information about the systems present in the vapor is in the first peak, corresponding to the bond lengths. The major component of the vapor, the monomer, has only one Cl⋯Cl nonbonded distance, but the clusters have many strong contributions in this region, even if they are present only in small amounts. Therefore, it is not surprising that depending on the refinement scheme, within a certain interval, different vapor compositions and somewhat different geometrical parameters can give equally good agreement—even if we consider only realistic solutions. Moreover, if we accept the results of the computation about the structure of the clusters, we have altogether eight different Cr–Cl bond lengths within the first peak, differing from each other by about 0.02 to 0.20 Å, with their different vibrational amplitudes and different weights depending on their relative amounts.

There is one more uncertainty concerning the ED results. Our computations showed (see Table 1, below) that the linear  ${}^5\Pi_g$  saddle-point state is only about 0.02–0.09 eV higher in energy than the  ${}^5B_2$  ground state, and this means that molecules in this state may also be present in the vapor phase, since the thermal energy of our experiment is more than enough to produce them. Even if the lifetime of these transition-state molecules is short, it might still be much longer than the very fast interaction time of the electron beam and the molecular beam in the experiment (approximately  $10^{-18}$  s). Even molecules in the  ${}^5\Sigma_g^+$  excited state might be present in the vapor according to some of the computations. The monomers in the  ${}^3\Pi_g$  and  ${}^3\Sigma_g^+$  states are linear and also have somewhat longer bond lengths than the ground-state ( ${}^5B_2$ ) molecule. We tried to include two different monomeric species in the analysis, but this was not successful due to the high correlations. There is also a certain elusiveness concerning the dimeric species which constitutes about 20% of the vapor. The energy difference, for example, between the nonet and singlet dimeric structures of  $C_{2v}$  symmetry is about 0.024 eV, and the DFT and CASPT2 methods do not even agree on which one is the ground state. These structures differ by several thousandths of an Å in some of their bond lengths. Moreover, the energy difference between the  $C_{2v}$  and  $C_{2h}$  symmetry dimers is only about 0.001 eV, although their geometries do not differ much. Therefore, in determining the uncertainties of the structural parameters, we have to take into consideration that some structures may be averages of similar molecular species.

## Results and Discussion

**The CrCl<sub>2</sub> monomer:** The results of the different-level computations on the CrCl<sub>2</sub> monomer are listed in Table 1 together with the available literature data. Experimental structural parameters are also included for comparison. Consider-

ing the linear geometries, from the three possible high-spin states,  ${}^5\Sigma_g^+$  ( $\delta_g^2, \pi_g^2$ ),  ${}^5\Pi_g$  ( $\delta_g^2, \pi_g^1, \sigma_g^1$ ), and  ${}^5\Delta_g$  ( $\delta_g^1, \pi_g^2, \sigma_g^1$ ), the  ${}^5\Pi_g$  state is the lowest in energy. However, the  ${}^5\Pi_g$  state is not a minimum; it is a transition state undergoing a Renner–Teller distortion<sup>[56,57]</sup> by splitting into two nondegenerate states, a  ${}^5B_2$  and an  ${}^5A_2$  state, of which the  ${}^5B_2$  state is the ground state (see Figure 3). The shape of the molecule

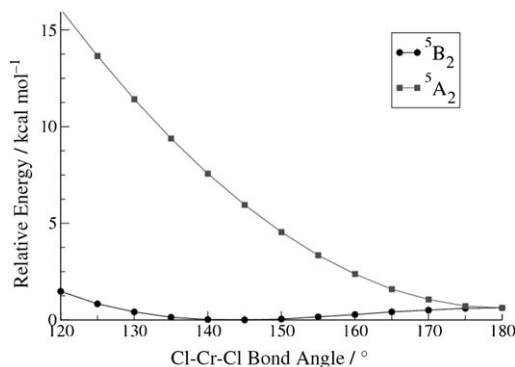


Figure 3. Bending potential curves of the  ${}^5B_2$  (lower curve) and  ${}^5A_2$  (upper curve) states obtained from B3PW91 calculations.

in the ground electronic state of CrCl<sub>2</sub> is bent. Note that the UKS-DFT calculations give only one imaginary vibrational mode instead of a doubly degenerate one for the  ${}^5\Pi_g$  state, which implies that the multireference character is not well described by the Kohn–Sham approach, and one may require partial occupations for the spin-orbitals to remedy this situation. A more accurate description of this state (and of the  ${}^5\Delta_g$  state as well) is obtained from a state-averaged CASSCF calculation in which the  $\pi_g$  (or  $\delta_g$ ) orbitals possess half occupancies in each orbital. Although our CASSCF-(16,15) treatment may lack major dynamic correlation, it also predicts a bent  ${}^5B_2$  ground-state structure, with the  ${}^5\Pi_g$  saddle point lying only 0.075 eV above the ground state. The next local minimum is of  ${}^5\Sigma_g^+$  symmetry, and about 0.15–0.28 eV above the  ${}^5B_2$  ground state. It was only the CASPT2 calculation that found the  ${}^5\Sigma_g^+$  state to be the ground state, but only by 0.035 eV below the  ${}^5B_2$  state. Even the single-reference coupled cluster treatment gives the  ${}^5B_2$  as the ground state, and we are quite confident that the correct ordering of the electronic states is  ${}^5B_2 < {}^5\Sigma_g^+ < {}^5\Delta_g$ . All other states of different spin multiplicity are considerably higher in energy and cannot be considered as contestants for the ground state of CrCl<sub>2</sub>. Nevertheless, we mention that unrestricted B3LYP describes reasonably well the singlet state, being 5.03 eV above the  ${}^5B_2$  state in reasonable agreement with our CCSD(T) value of 4.28 eV.

The  ${}^5B_2$  ground electronic state shows a very shallow bending potential with a bond angle of between 144° (B3LYP) and 168° (CASPT2) and only less than 0.1 eV below the linear high-symmetry point. Hence, it is difficult to predict an accurate bond angle for the  ${}^5B_2$  state. Note that for CaF<sub>2</sub>, which has a very shallow bending mode as well,<sup>[58]</sup> a bent structure was identified in the gas phase as

Table 1. Relative energies, geometrical parameters, and vibrational frequencies of CrCl<sub>2</sub> in different electronic states. Energies in eV, distances in Å, angles in degrees, and frequencies in cm<sup>-1</sup>.

State	Method <sup>[a]</sup>	Ref. <sup>[b]</sup>	$\Delta E$	$R(\text{CrCl})$	$\angle(\text{ClCrCl})$	$\nu_{\text{bend}}^{\text{[c]}}$	$\nu_{\text{sym-str}}$	$\nu_{\text{asym-str}}$	
<sup>5</sup> B <sub>2</sub>	exptl(IR)	[5,9]	–	–	–	–	–	493.5 <sup>[d]</sup> , 457.4 <sup>[e]</sup>	
		[7,8]	–	–	–	–	–	475 <sup>[f]</sup> , 458.5 <sup>[g]</sup>	
		[12]	–	–	–	–	–	422 <sup>[h]</sup>	
	exptl(ED)		–	2.196(20)	149(10)	–	–	–	
	B3LYP		0	2.193	146.7	49.3	349.4	472.8	
	MP2 <sup>[i]</sup>		0	2.179	165.2	24.8	339.3	496.9	
	B3PW91 <sup>[i]</sup>		0	2.175	143.6	56.8	357.6	476.7	
	CCSD(T)		0	2.194	167.0	32.4	337.9	492.2	
	CASPT2		0.035	2.201	167.5	–	–	–	
	CASSCF <sup>[j]</sup>		0	2.193	146.7	–	–	–	
<sup>5</sup> Π <sub>g</sub>	B3LYP	[22]	0	2.201	144.3	57.2	344.2	467.3	
	CCSD(T)	[23]	0	2.199	156.2	45	338	486	
	B3LYP		0.020	2.198	180	47.4i/92.4 <sup>[k]</sup>	329.6	479.0	
	MP2 <sup>[i]</sup>		0.001	2.181	180	18.0i/101.3 <sup>[k]</sup>	334.6	497.4	
	B3PW91 <sup>[i]</sup>		0.027	2.182	180	46.2i/98.1 <sup>[k]</sup>	334.1	484.5	
	CCSD(T)		0.032	2.194	180	–	–	–	
	CASPT2		0.085	2.202	180	–	–	–	
	CASSCF <sup>[j]</sup>		0.075	2.198	180	–	–	–	
	CASSCF	[55]	–	2.175	180	–	–	–	
	B3LYP	[22]	0.012	2.209	180	–	–	–	
<sup>5</sup> Σ <sub>g</sub> <sup>+</sup>	BP-VWN	[20]	–	2.173	180	[i,k]	358	476	
	LSDA	[21]	0	2.15	180	85	315	480	
	HF	[19]	0.282	2.309	180	–	–	–	
	B3LYP		0.156	2.239	180	69.7	327.7	460.3	
	CCSD(T)		0.145	2.240	180	80.8	333.5	474.8	
	CASPT2		0	2.240	180	–	–	–	
	CASSCF <sup>[j]</sup>		0.276	2.239	180	–	–	–	
	B3LYP	[22]	0.200	2.248	180	–	–	–	
	BP-VWN	[20]	–	2.216	180	–	–	–	
	HF	[19]	0	2.315	180	–	–	–	
<sup>5</sup> Δ <sub>g</sub>	LSDA	[21]	0.532	2.21	180	65	326	465	
	B3LYP		0.804	2.226	180	49.9	322.5	468.9	
	CCSD(T)		0.765	2.228	180	–	–	–	
	CASSCF		0.910	2.226	180	–	–	–	
	CASPT2		0.654	2.229	180	–	–	–	
	CASSCF <sup>[j]</sup>		0.910	2.226	180	–	–	–	
	B3LYP	[22]	0.860	2.237	180	–	–	–	
	LSDA	[21]	1.039	2.183	180	56	325	459	
	B3LYP		1.636	2.135	180	19.8	352.1	510.0	
	CCSD(T)		1.794	2.122	180	–	–	–	
<sup>3</sup> Σ <sub>g</sub> <sup>-</sup>	CASPT2		2.319	2.158	180	–	–	–	
	BP-VWN	[20]	–	2.101	180	–	–	–	
	LSDA	[21]	0.899	2.078	180	90	348	540	
	B3LYP		5.025	2.144	180	51.7	367.8	508.5	
	CCSD(T)		4.284	2.170	180	–	–	–	
	CASPT2		3.503	2.138	180	–	–	–	
	BP-VWN	[20]	–	2.126	180	–	–	–	
	<sup>1</sup> Σ <sub>g</sub> <sup>+</sup>								

[a] Unless otherwise mentioned, a CASSCF(4,5) was used. Unless otherwise noted, an aug-cc-pVDZ basis for Cl was used. [b] Unless otherwise stated, the data given are from this study. [c] For the linear structures, the bending mode is doubly degenerate. [d] MI-IR (Ar) from ref. [5]. [e] MI-IR (Ar) from ref. [9]. [f] Gas-phase IR data from ref. [8]. [g] MI-IR (Ar) from ref. [7]. [h] Gas-phase IR from ref. [12]. [i] cc-pVTZ basis set used for Cl. [j] A CASSCF(16,15) was used. [k] *i* indicates imaginary frequency in the bending mode.

this molecule has a nonzero dipole moment.<sup>[59]</sup> The B3LYP and CCSD(T) geometry optimization produces a bond length of 2.193 and 2.194 Å, respectively, in excellent agreement with the estimated experimental equilibrium bond length of 2.196(20) Å. The CASPT2(4,5) result is 2.201 Å, also in very good agreement. It is known that the MP2 method tends to underestimate bond lengths. B3PW91 also gives a bond length too short, and two other DFT studies determined similarly short bond lengths.<sup>[20,21]</sup> Note that the

difference in bond lengths between the <sup>5</sup>Π<sub>g</sub> saddle point and the <sup>5</sup>B<sub>2</sub> minimum structure is very small.

The results of the ED analysis are given in Table 2. The thermal average bond length ( $r_g$ ) of 2.214(13) Å agrees with the previously<sup>[3]</sup> determined value within their uncertainties. The equilibrium bond length can be estimated from the  $r_g$  parameter by introducing vibrational corrections. As discussed in the ED analysis section above, the value we determined here depends on several assumptions and thus carries a larger than usual uncertainty. The equilibrium Cr–Cl bond length ( $r_e^M$ ) of 2.196(20) Å is in agreement with several of our computed values, see Table 1. The bond angle from electron diffraction, 149(10)°, has an even larger uncertainty, due to the fact that the peak around 4.2 Å on the radial distribution curve has several components from the dimers and trimers, and thus the exact position of the monomer Cl⋯Cl distance is uncertain. Nonetheless, this bond angle does not correspond to a linear molecule, even if taking into account the shrinkage effect. If we assume that due to the high experimental temperature and the small energy difference between the ground state and the <sup>5</sup>Π<sub>g</sub> state the linear transition-state molecules could also be present in the vapor in a smaller amount—and assuming that they had a bond length similar to that of the ground-state molecule as obtained from our calculations

(see Table 1)—its Cl⋯Cl distance would be only about 0.12 Å longer than that of the ground-state molecule with a 149° bond angle due to the shrinkage effect. This would somewhat decrease the Cl⋯Cl distance and, consequently, the bond angle of the ground-state molecule. The large uncertainty of the bond angle covers this possibility. Moreover, the energy difference between the <sup>5</sup>B<sub>2</sub> and <sup>5</sup>Π<sub>g</sub> states is only 0.020 eV, or about 161 cm<sup>-1</sup>. For the bending mode, the harmonic zero-point vibrational energy ( $E_0$ ) is ap-

Table 2. Geometrical parameters and vapor composition from electron diffraction.

Parameter	Value
$r_g(\text{Cr}-\text{Cl})^{[a]}$ [Å]	2.214(13)
$r_e^M(\text{Cr}-\text{Cl})^{[b]}$ [Å]	2.196(20)
$l(\text{Cr}-\text{Cl})^{[c]}$ [Å]	0.093(3)
$\kappa(\text{Cr}-\text{Cl})^{[d]}$ [Å <sup>-3</sup> ]	$5.17 \times 10^{-5}$
$r_g(\text{Cl}\cdots\text{Cl})$ [Å]	4.272(95)
$l(\text{Cl}\cdots\text{Cl})$ [Å]	0.216(26)
$\angle_a \text{Cl}-\text{Cr}-\text{Cl}$ [°]	149(10)
monomer [%]	77.4(4.2)
dimer [%]	18.7(4.2)
trimer [%]	3.9(2.8)

[a] The  $r_g(\text{Cr}-\text{Cl})$  value from ref. [3] is 2.207(10) Å. [b] Calculated from  $r_g(\text{Cr}-\text{Cl})$  by anharmonic corrections. [c] Refined in a group with the amplitudes of the dimer and trimer bond lengths. [d] Not refined.

proximately 25 cm<sup>-1</sup>, and the bending mode has only three vibrational states within the energy well (25, 75 and 125 cm<sup>-1</sup>). If we take a Boltzmann distribution over 66 states including the ground state (i.e., taking the states ranging from 25–3275 cm<sup>-1</sup>) at 1200 K, we calculate that only 16% of the monomers will be within the first three bending states. Hence, 84% of the monomers will have enough energy to become linear, which is best described as a dynamic Renner–Teller system.

The electronic absorption spectra of CrCl<sub>2</sub>, reported by DeKock and Gruen<sup>[16]</sup> contains two transitions located at 5400 and 9000 cm<sup>-1</sup>. The oscillator strengths of these two transitions indicate that they arise from Laporte forbidden d<sup>4</sup>→d<sup>4</sup> transitions. These type of transitions are indicative of a linear geometry which occur between the states of  $D_{\infty h}$  symmetry. Based on ligand-field theory, DeKock and Gruen assigned these two transitions to  $^5\Sigma_g^+ \rightarrow ^5\Pi_g$  and  $^5\Sigma_g^+ \rightarrow ^5\Delta_g$ , respectively. Because ligand-field theory incorrectly predicts the relative energies of the 3d metal orbitals, the assignment of the first transition is incorrect, as the  $^5\Pi_g$  state is lower in energy than the  $^5\Sigma_g^+$  state. Furthermore, the  $^5\Pi_g \rightarrow ^5\Sigma_g^+$  transition is calculated to be at 911 cm<sup>-1</sup> at the CCSD(T) level, which is well below both excitation energies. The 5400 cm<sup>-1</sup> transition is close to our calculated  $^5\Pi_g^+ \rightarrow ^5\Delta_g$  transition, which is at 5912 cm<sup>-1</sup> at the CCSD(T) level (not including zero-point vibrational effects). None of the transitions studied for CrCl<sub>2</sub> came close to the 9000 cm<sup>-1</sup> transition, and it was predicted that this band could have arisen from transitions between rotational–vibrational levels of the  $^5\Pi_g$  and  $^5\Delta_g$  states.<sup>[22]</sup> This is rather unlikely according to our results, but multireference configuration interaction calculations are needed to identify these bands (for a recent multireference treatment of CrO<sub>2</sub> see reference [60]).

Mulliken and NBO analyses at the B3LYP level of theory were also carried out for the lowest energy species and the results are given in Table 3. The charges and spin densities obtained at the B3PW91 level of theory are very similar and are therefore omitted. It is apparent that in the high-spin state the spin density is almost exclusively located at the Cr atom, with only a very small amount of spin density situated at the chlorine atoms. The charges between the different

Table 3. Results of Mulliken and NBO analyses for the lowest energy species from B3LYP calculations.

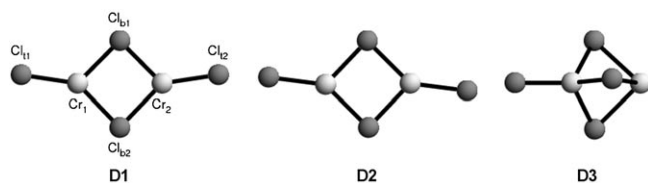
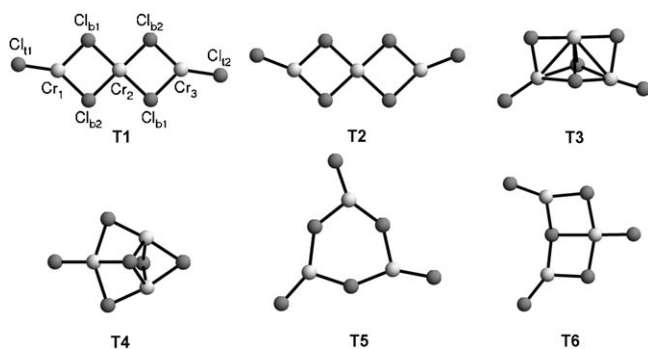
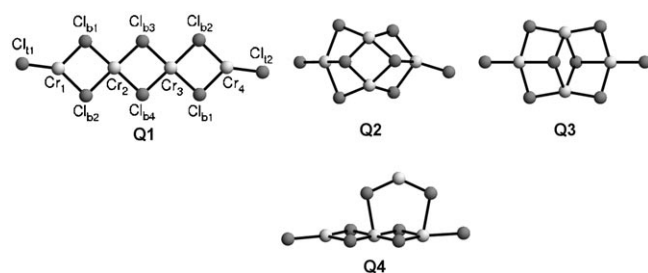
Species	State	Atom	Mulliken charge	NBO charge	Mulliken spin density		
monomer	$^5B_2$	Cr	0.427	1.153	4.085		
		Cl	-0.213	-0.577	-0.042		
	$^5\Pi_g$	Cr	0.435	1.166	4.132		
		Cl	-0.218	-0.583	-0.066		
	$^5\Sigma_g^+$	Cr	0.561	1.386	3.964		
		Cl	-0.280	-0.693	0.018		
	$^5\Delta_g$	Cr	0.470	1.338	3.926		
		Cl	-0.235	-0.669	0.037		
	$^3\Sigma_g^-$	Cr	0.392	0.878	2.228		
		Cl	-0.196	-0.439	-0.114		
	$^1\Sigma_g^+$	Cr	0.315	0.879	0		
		Cl	-0.157	-0.439	0		
dimer	$^1A_1$	Cr <sub>1</sub>	0.396	1.111	-4.063		
		Cr <sub>2</sub>	0.396	1.111	4.063		
		Cl <sub>1</sub>	-0.308	-0.568	0.011		
		Cl <sub>2</sub>	-0.308	-0.568	-0.011		
		Cl <sub>b1</sub>	-0.114	-0.559	0		
		Cl <sub>b2</sub>	-0.063	-0.526	0		
	$^9A_1$	Cr <sub>1</sub> ,Cr <sub>2</sub>	0.410	1.134	4.081		
		Cl <sub>1</sub> ,Cl <sub>2</sub>	-0.312	-0.578	-0.013		
		Cl <sub>b1</sub>	-0.143	-0.587	-0.060		
		Cl <sub>b2</sub>	-0.052	-0.525	-0.077		
		trimer	$^5A_g$	Cr <sub>1</sub> ,Cr <sub>3</sub>	0.603	1.122	4.059
				Cr <sub>2</sub>	-0.022	0.994	-4.153
Cl <sub>1</sub> ,Cl <sub>2</sub>	-0.352			-0.579	-0.005		
$^1A_g$	Cl <sub>b1</sub>		-0.100	-0.511	0.013		
	Cl <sub>b2</sub>		-0.140	-0.529	0.010		
	tetramer		$^1A_g$	Cr <sub>1</sub> ,Cr <sub>4</sub>	0.782	1.122	-4.031
Cr <sub>2</sub> ,Cr <sub>3</sub>		0.021		0.999	4.155		
Cl <sub>1</sub> ,Cl <sub>2</sub>		-0.362		-0.581	0.003		
$^3A_1$		Cl <sub>b1</sub>	-0.136	-0.513	-0.014		
		Cl <sub>b2</sub>	-0.174	-0.530	-0.011		
		Cl <sub>b3</sub> ,Cl <sub>b4</sub>	-0.131	-0.498	-0.102		

electronic states vary only little. However, the Mulliken and NBO charges differ significantly, the latter indicating a charge at Cr two to three times larger than the Mulliken analysis. However, both methods indicate that even though the molecule is ionic, there is substantial covalent character. The data given in Table 4 show a Wiberg bond index of about 0.64 for the Cr–Cl bond in the  $^5B_2$  state, thus supporting this observation.

**CrCl<sub>2</sub> clusters:** As mentioned in the Computational methods section, we searched for the global minimum for the dimer Cr<sub>2</sub>Cl<sub>4</sub> (denoted as **D** in the following), the trimer Cr<sub>3</sub>Cl<sub>6</sub> (**T**), and the tetramer Cr<sub>4</sub>Cl<sub>8</sub> (**Q**). The lowest-energy structures are shown in Figures 4–6. Irrespective of the spin-state, we obtain planar, doubly bridged CrCl<sub>2</sub> units as the global minimum. These planar chain structures of CrCl<sub>2</sub> units are the basic building blocks of the  $\alpha$ -CrCl<sub>2</sub> phase in the solid state.<sup>[31,61,62]</sup> In the solid, every Cr atom is in a ligand field of an elongated and distorted octahedron of Cl atoms.<sup>[61,62]</sup> However, four Cl atoms form a close rectangle with the Cr atom in its centre, resulting in CrCl<sub>2</sub> chains along the crystallographic *c*-axis. The global minima of the dimers, trimers, and tetramers (**D1**, **T1**, and **Q1**, respectively) as shown in Figures 4–6 are the basic units of these chains. In our pre-

Table 4. Wiberg bond indices for the lowest energy species from B3LYP calculations.

Species	State	Bond	Wiberg bond index
monomer	$^3B_2$	Cr–Cl	0.642
	$^5\Pi_g$	Cr–Cl	0.634
	$^5\Sigma_g^+$	Cr–Cl	0.495
	$^5\Delta_g$	Cr–Cl	0.458
	$^3\Sigma_g^-$	Cr–Cl	0.944
dimer	$^1A_1$	Cr–Cl	0.917
		Cr <sub>1</sub> –Cl <sub>t1</sub>	0.639
		Cr <sub>1</sub> –Cl <sub>b1</sub>	0.338
	$^9A_1$	Cr <sub>1</sub> –Cl <sub>b2</sub>	0.372
		Cr <sub>1</sub> –Cl <sub>t1</sub>	0.624
trimer	$^5A_g$	Cr <sub>1</sub> –Cl <sub>b1</sub>	0.315
		Cr <sub>1</sub> –Cl <sub>b2</sub>	0.377
		Cr <sub>1</sub> –Cl <sub>t1</sub>	0.623
		Cr <sub>1</sub> –Cl <sub>b1</sub>	0.377
		Cr <sub>1</sub> –Cl <sub>b2</sub>	0.340
tetramer	$^1A_g$	Cr <sub>2</sub> –Cl <sub>b1</sub>	0.372
		Cr <sub>2</sub> –Cl <sub>b2</sub>	0.371
		Cr <sub>1</sub> –Cl <sub>t1</sub>	0.620
		Cr <sub>1</sub> –Cl <sub>b1</sub>	0.378
		Cr <sub>1</sub> –Cl <sub>b2</sub>	0.343
		Cr <sub>2</sub> –Cl <sub>b1</sub>	0.367
		Cr <sub>2</sub> –Cl <sub>b2</sub>	0.365
		Cr <sub>2</sub> –Cl <sub>b3</sub>	0.376
		Cr <sub>2</sub> –Cl <sub>b4</sub>	0.375

Figure 4. Low-energy minima for the CrCl<sub>2</sub> dimer.Figure 5. Low-energy minima for the CrCl<sub>2</sub> trimer.Figure 6. Low-energy minima for the CrCl<sub>2</sub> tetramer.

liminary calculations, we found two structures close in energy with the terminal Cl atoms (denoted as Cl<sub>t</sub>) either in *cis* ( $C_{2v}$  symmetry) or in *trans* ( $C_{2h}$  symmetry) position to the chain, that is, structures **D1**, **D2** and **T1**, **T2**. However, extended basis set calculations only gave the *trans* structures as minima for the trimer and the tetramer.

The high-symmetry  $D_{2h}$ -bridged structures, quite common for metal dihalide dimers,<sup>[2]</sup> represent only saddle points with two imaginary frequencies for the bending of the terminal Cl atoms towards *trans* minima. This is the result of a pseudo Jahn–Teller distortion, with one mode, for example of  $B_{3g}$  symmetry, towards the *trans* structure. Structures which include Cr–Cr bonds are found to be too high in energy to be considered here. We show a few high energy structures in Figures 4–6, obtained at the PW91/LanL2DZ level of theory; **D3** (0.519 eV above the global minimum), **T3**, **T4**, **T5**, and **T6** (0.445, 0.697, 0.945, and 0.976 eV above the global minimum structure, respectively), and **Q2**, **Q3**, and **Q4** (0.852, 0.864, and 0.934 eV above the global minimum structure, respectively). They all consist of (more or less) bent CrCl<sub>2</sub> units. As they are not a major component in the gas phase even at higher temperature, they will not be discussed further.

Based on the lowest energy structures for all oligomers studied here, our results clearly indicate that the chain motif found in the solid structure can already be seen in the earliest process of CrCl<sub>2</sub> nucleation. Our DFT calculations also show that as the size of the chain increases, the average Cr–Cl<sub>b</sub> distances in the oligomers converge towards a value that is quite close to the experimental solid-state intrachain Cr–Cl distance of Oswald<sup>[61]</sup> (Figure 7). Note that the *trans* minimum structures are ideally aligned for nucleation towards the one-dimensional CrCl<sub>2</sub> chain.

The electron diffraction radial distribution curve (Figure 2) clearly indicates that there are other species present in the gas phase beside the monomer, since for a triatomic molecule only two peaks corresponding to the Cr–Cl

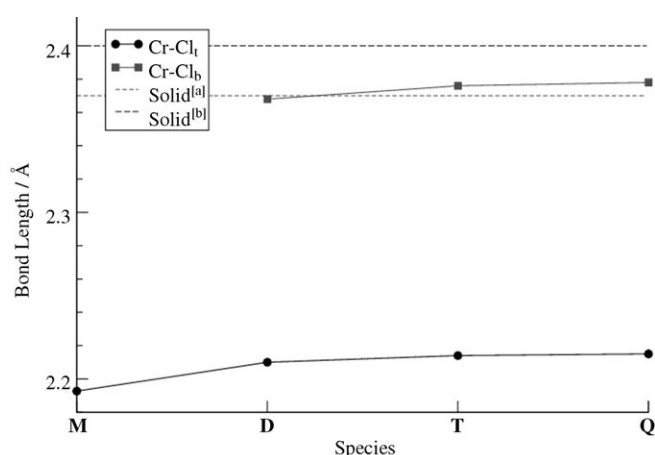


Figure 7. Average Cr–Cl<sub>b</sub> and Cr–Cl<sub>t</sub> distances for the different CrCl<sub>2</sub> oligomers from B3LYP calculations. The experimental solid-state intrachain Cr–Cl values are shown as dashed lines. [a] From X-ray data of Oswald (2.37 Å).<sup>[61]</sup> [b] From X-ray data of Tracy (2.4 Å).<sup>[62]</sup>



bond length and the Cl...Cl nonbonded distance would be observed. The peak at 3.3 Å contains the Cr...Cr and Cl<sub>b</sub>...Cl<sub>b</sub> distances within the rings of the oligomers (Figure 2). The monomer Cl...Cl distance is in the peak at 4.3 Å, together with several oligomer distances and the further peaks, at about 5.4 and 7.3 Å, correspond to different longer nonbonded distances of the dimer and trimer molecules. The agreement between the experimental and calculated distribution is very good, demonstrating that the chain-like structures support the experimental data. We also have to mention that the more general, six-membered ring structure (**T5**) of metal halide trimers (see, for example reference [63]) does not agree with the experimental data. In that structure, there are three equal Cr...Cr distances in the ring that are situated around 4.0–4.1 Å. That would push the monomer Cl...Cl distance to the peak at 3.3 Å, resulting in a monomer bond angle smaller than 110 degrees, which would not agree with either of our computations. Even if the trimer amount is about 3% in both types of refinements, due to the large atomic number of Cr and the fact that there are three such distances, its effect is noticeable. Due to the many closely spaced distances and to the relatively low concentration of the larger species in the vapor, it is not possible to distinguish between their high-spin and low-spin states, or between the C<sub>2v</sub> and C<sub>2h</sub> structures of the dimer.

The most important structural parameters of the clusters are listed in Table 5, all other distances and angles can be derived from the Cartesian coordinates given in Table S2 (Supporting Information). The different spin states for a

specific cluster differ only little in energy, and also have very similar geometries. The terminal Cr–Cl bond lengths are about the same in the low- and high-spin structures, while the bridging bonds are more affected by the change in spin multiplicity than the terminal Cr–Cl bonds. The difference between the geometries of the *cis* C<sub>2v</sub> and *trans* C<sub>2h</sub> structures of the dimers in the same electronic states is also very small. The B3PW91 functional together with the better triple-zeta basis set on chlorine gave considerably shorter bond lengths by about 0.02 Å with respect to the B3LYP functional with the double-zeta basis set on chlorine. We mention that the NBO analysis gave no evidence for Cr–Cr bonding in the clusters.

In the solid state, the spins of the Cr 3d electrons are found to be antiferromagnetically coupled with four parallel spins situated almost exclusively in the d-bands of Cr along these chains, which is well described by the Ising spin-coupling model.<sup>[64,65]</sup> However, the energy difference between the antiferromagnetic (AFM) and the ferromagnetic (FM) phase is very small, with only 0.016 eV per CrCl<sub>2</sub> unit,<sup>[31]</sup> indicating little direct spin coupling between the Cr atoms. We therefore expect that the low- and high-spin states are close in energy for the clusters as well. According to Hund's rule, one expects the high-spin states to be more stable than the low-spin states. However, in the solid the AFM state is the ground state,<sup>[31]</sup> and that would predict a low-spin singlet state for the dimer and the tetramer, and a quintet state for the trimer for the CrCl<sub>2</sub> clusters. This is, indeed, the case. According to our B3LYP (B3PW91) calculations, the global

Table 5. Molecular properties for the global minimum structures of CrCl<sub>2</sub> clusters for different spin states.<sup>[a]</sup>

Property	Method	<b>D1</b>		<b>D2</b>		<b>T1</b>		<b>Q1</b>		
		<sup>1</sup> A <sub>1</sub>	<sup>9</sup> A <sub>1</sub>	<sup>1</sup> A <sub>g</sub>	<sup>9</sup> A <sub>g</sub>	<sup>5</sup> A <sub>g</sub>	<sup>13</sup> A <sub>g</sub>	<sup>1</sup> A <sub>g</sub>	<sup>9</sup> A <sub>g</sub>	<sup>17</sup> A <sub>g</sub>
<i>D<sub>e</sub></i>	PW91 <sup>[b]</sup>	47.8	47.2	47.8	47.2	96.1	95.4	143.9	143.4	143.0
	PW91 <sup>[c]</sup>	45.4	45.1	45.6	45.1	87.8	84.2	131.9	–	127.1
	B3LYP	46.6	45.3	46.5	45.2	90.8	89.7	135.0	134.6	133.9
	B3PW91	47.1	46.0	47.0	45.8	92.6	91.6	138.8	137.5	137.1
<i>D<sub>e</sub></i> + ZPVE	B3LYP	45.6	44.4	45.6	44.3	88.9	87.8	132.2	131.7	131.1
	B3PW91	46.1	45.0	46.1	44.8	90.7	89.6	135.4	134.6	134.2
<i>R</i> (Cr <sub>1</sub> –Cl <sub>1t</sub> )	B3LYP	2.210	2.211	2.210	2.211	2.214	2.215	2.215	2.216	2.216
	B3PW91	2.193	2.195	2.193	2.195	2.198	2.198	2.199	2.198	2.200
<i>R</i> (Cr <sub>1</sub> –Cl <sub>1b</sub> )	B3LYP	2.354	2.355	2.353	2.362	2.348	2.353	2.348	2.349	2.352
	B3PW91	2.327	2.330	2.328	2.339	2.322	2.328	2.322	2.324	2.327
<i>R</i> (Cr <sub>1</sub> –Cl <sub>1b2</sub> )	B3LYP	2.373	2.389	2.372	2.386	2.366	2.372	2.364	2.374	2.370
	B3PW91	2.360	2.377	2.358	2.370	2.352	2.360	2.351	2.353	2.357
<i>R</i> (Cr <sub>2</sub> –Cl <sub>1b</sub> )	B3LYP	2.354	2.355	2.372	2.386	2.391	2.393	2.392	2.398	2.397
	B3PW91	2.327	2.330	2.358	2.370	2.370	2.372	2.373	2.372	2.376
<i>R</i> (Cr <sub>2</sub> –Cl <sub>1b2</sub> )	B3LYP	2.373	2.389	2.353	2.362	2.391	2.395	2.392	2.400	2.400
	B3PW91	2.360	2.377	2.328	2.339	2.370	2.375	2.374	2.374	2.380
<i>R</i> (Cr <sub>2</sub> –Cl <sub>1b3</sub> )	B3LYP	–	–	–	–	–	–	2.384	2.377	2.382
	B3PW91	–	–	–	–	–	–	2.361	2.361	2.362
<i>R</i> (Cr <sub>2</sub> –Cl <sub>1b4</sub> )	B3LYP	–	–	–	–	–	–	2.384	2.378	2.383
	B3PW91	–	–	–	–	–	–	2.362	2.370	2.364
<i>R</i> (Cr <sub>1</sub> –Cr <sub>2</sub> )	B3LYP	3.307	3.384	3.307	3.394	3.390	3.432	3.383	3.412	3.435
	B3PW91	3.257	3.346	3.258	3.364	3.346	3.399	3.342	3.376	3.402
∠(Cl <sub>1t</sub> –Cr <sub>1</sub> –Cl <sub>1b</sub> )	B3LYP	125.9	122.9	125.9	124.0	126.6	127.0	126.9	126.5	127.5
	B3PW91	120.4	118.6	120.5	120.7	121.4	121.9	121.5	121.8	122.0
∠(Cl <sub>1b</sub> –Cr <sub>1</sub> –Cl <sub>1b2</sub> )	B3LYP	91.2	89.0	91.2	88.7	89.7	88.4	90.0	88.5	88.5
	B3PW91	91.9	89.4	91.9	88.8	90.2	88.5	90.5	89.3	88.6

[a] Dissociation energies *D<sub>e</sub>* in kcalmol<sup>-1</sup>, distances in Å, and angles in degrees. For the different structures **D1**, **D2**, **T1** and **Q1** see Figures 4–6. [b] PW91 calculations using the LanL2DZ basis set. [c] PW91 calculations using PAW method and plane wave basis sets.

minimum is the singlet **D1** structure of the dimer, the quintet structure **T1** for the trimer, and the singlet structure **Q1** of the tetramer (see Table 5). Furthermore, based on our results for the different spin-states of the monomer, which resulted in a  $^5B_2$  state as the ground state, we only had to couple total spin  $S=2$  monomer units to build up successively the chain structure to the solid phase of  $\text{CrCl}_2$ . This results in the AFM singlet ( $S=0$ ) and FM nonet states for the dimer ( $S=4$ ), the AFM quintet ( $S=2$ ) and the FM tri-decet ( $S=6$ ) states for the trimer, and the AFM singlet ( $S=0$ ), the intermediate nonet ( $S=4$ ), and the FM septendecet ( $S=8$ ) states for the tetramer.

This analysis is supported by the Mulliken spin densities shown in Table 3. For the monomer the spin density is almost exclusively situated at the Cr atom with four unpaired electrons ( $S=2$ ). Unfortunately, one of the shortcomings of BS-DFT is that it does not describe coupled spin states well when two or more transition-metal centers are within close proximity.<sup>[30]</sup> The uncoupled, high-spin state of the dimer ( $\uparrow\uparrow$ ) is described reasonably well with DFT. However, we get either the ( $\uparrow\downarrow$ ) or ( $\downarrow\uparrow$ ) configuration instead of the correct ( $\uparrow\downarrow-\downarrow\uparrow$ ) combination for the singlet state of the dimer. Ideally, the singlet state should have zero net spin density everywhere in the molecule for even sized clusters; however, the BS solution has an excess of  $\alpha$  and  $\beta$  spin density located on the adjacent Cr atoms. These BS solutions are also seen in the trimer and tetramer. The coupling for the trimer consists of an oscillating ( $4\alpha, 4\beta, 4\alpha$ ) pattern for the quintet state, and the coupling pattern for the singlet tetramer consists of ( $4\beta, 4\alpha, 4\alpha, 4\beta$ ). The nonet state for the tetramer is slightly different, with the coupling pattern being ( $4\alpha, 2\beta, 2\beta, 4\alpha$ ). The primary disadvantage of BS-DFT is that the exchange coupling between the metal centers is overestimated, and the coupled-spin states are overstabilized.<sup>[66]</sup>

In light of the BS solutions for the low-spin states of the clusters, CASPT2(8,10) calculations were performed for the singlet- and nonet-optimized B3LYP structures of **D1** in order to determine whether the energy differences are, indeed, that small. Not surprisingly, restricted Hartree–Fock calculations predict a nonet ground state with the singlet state lying very high in energy, 8.50 eV. The singlet energy drops substantially at the unrestricted Hartree–Fock level and the difference becomes only 0.02 eV. At the CASSCF-(8,10) level of theory, the singlet state lies only 0.089 eV above the nonet state. This energy difference decreases further to 0.024 eV at the CASPT2 level of theory. CASPT2 calculations, therefore, predict that the high-spin dimer is the lowest in energy. However, these calculations have been performed at the B3LYP optimized geometry as the CASPT2 optimization would be computationally too demanding, and a proper geometry optimization could easily favor the singlet over the nonet state.

The calculated dissociation energies into  $\text{CrCl}_2$  units at the PW91, B3LYP, and B3PW91 level of theory are shown in Table 5. The results show that the addition of each  $\text{CrCl}_2$  unit to the  $\text{CrCl}_2$  chain brings an almost constant energy gain of about 45 kcal mol<sup>-1</sup>. This is also supported by our

PAW calculations with which we obtain a cohesive energy of 42.9 kcal mol<sup>-1</sup> per  $\text{CrCl}_2$  unit for the AFM infinite chain. This compares well with the 46.4 kcal mol<sup>-1</sup> per unit for the solid, which includes interactions between the  $\text{CrCl}_2$  chains. Somewhat higher energies are obtained with wavefunction based methods. At the unrestricted (single-reference) MP2 level of theory, we calculate a dissociation energy for structure **D1** of 57.4 kcal mol<sup>-1</sup> for the nonet state. In comparison, at the CASPT2 level we get 54.0 kcal mol<sup>-1</sup>. Hence we assume that the dissociation energies are underestimated by our DFT methods. We also considered the basis set superposition error (BSSE) from two-body contributions for the cluster formation. From the B3LYP calculations, the BSSE for the lowest energy clusters is 1.6 kcal mol<sup>-1</sup> for the dimer, trimer, and the tetramer, respectively. Apparently, they remain almost constant as the cluster size increases. The actual magnitude of BSSE is comparable or even larger than the energy difference between the low- and high-spin states; however, the BSSE does not change between the different spin states as we included only two-body terms.

A listing of the harmonic vibrational frequencies and IR intensities for the global minima structures of the monomeric up to the trimeric species are given in Table 6 from two

Table 6. Vibrational frequencies ( $\nu$ ) and IR intensities ( $I$ ) calculated for the global minima singlet or quintet states of the  $\text{CrCl}_2$  species.<sup>[a]</sup>

Method	Species	$\nu$ [cm <sup>-1</sup> ] ( $I$ [km mol <sup>-1</sup> ])
B3LYP	monomer	49(15), 349(11), 473(147)
B3PW91	monomer	57(14), 358(13), 477(136)
B3LYP	dimer	21(8), 23(2), 37, 90, 113, 115(19), 265(8), 282(6), 284, 330(46), 420(293), 433(5)
B3PW91	dimer	21(2), 30(8), 51, 90, 110, 115(19), 264(7), 287, 294(7), 339(43), 423(275), 437(13)
B3LYP	trimer	13(2), 18(7), 23, 29, 29, 90, 92(4), 95(8), 105, 133(18), 144, 213, 261, 281(13)
B3PW91	trimer	288, 293(5), 309, 330(191), 350(79), 424(299), 429, 12(1), 26, 27(7), 30, 37, 90, 96(9), 97(4), 104, 133(18), 139, 220, 265, 283(11)
		290, 303(4), 319, 336(182), 358(74), 428(293), 432

[a] Only non-zero intensities are listed and set in parentheses after the corresponding frequency.

different levels of computations. As expected, the most intense IR band for the monomer arises from the asymmetric Cr–Cl  $\nu_3$  stretching mode. The two DFT calculations predict this mode to occur at 473 and 477 cm<sup>-1</sup>, respectively, while MP2 and CCSD(T) calculations give 497 and 493 cm<sup>-1</sup>, respectively. The experimental information for this mode is rather confusing. Kobra assigned 475 cm<sup>-1</sup> to the asymmetric stretching frequency in a gas-phase IR experiment.<sup>[8]</sup> From the three available argon-matrix IR measurements, two groups assigned this mode similarly, at 458<sup>[7]</sup> and 457 cm<sup>-1</sup>,<sup>[9]</sup> while the third group assigned a value that is 40 cm<sup>-1</sup> higher, that is, 494 cm<sup>-1</sup>.<sup>[5]</sup> To make the picture more complicated, Hastie et al.<sup>[7]</sup> measured  $\text{CrCl}_2$  in a neon matrix and found the mode at 493 cm<sup>-1</sup>. Even taking into account matrix shifts, the 40 cm<sup>-1</sup> difference between the different matrices is too large—not to mention the difference be-

tween data referring to the same matrix. The picture is further complicated by a relatively new gas-phase measurement that suggested a  $422\text{ cm}^{-1}$  value for the asymmetric stretching frequency of  $\text{CrCl}_2$ .<sup>[10]</sup> We note that this frequency fits rather well to our most intense stretching frequency for the  $\text{CrCl}_2$  dimer.

Beside the evident problems of both high-temperature gas-phase and matrix-isolation IR experiments, including an uncertain amount of dimeric or other polymeric species, there are also other uncertainties in the experiments. For example, in two of them<sup>[9,10]</sup>  $\text{CrCl}_3$  was evaporated, not  $\text{CrCl}_2$  and thus the vapor composition was, possibly, even more complicated. In another experiment<sup>[5]</sup> metallic chromium was treated with chlorine gas at high temperature in argon atmosphere and the vapor composition was not checked.

In trying to decide which one of the measured frequencies could be the real gas-phase asymmetric stretching frequency of  $\text{CrCl}_2$ , it is worthwhile to compare this value to the asymmetric stretching frequencies of the other first-row transition-metal dihalides.<sup>[2]</sup> They change from about  $480\text{ cm}^{-1}$  ( $\text{MnCl}_2$ ) up to about  $520\text{ cm}^{-1}$  ( $\text{NiCl}_2$ ). Although there is no direct connection between the bond length and the  $\nu_3$  frequency, it is still worthwhile mentioning that the bond length is largest for  $\text{MnCl}_2$  ( $d^5$  electronic configuration), and it decreases toward  $\text{NiCl}_2$ ; the difference between the two being as large as  $0.13\text{ \AA}$ . Considering the position of Cr in the row, the  $\nu_3$  value around  $475\text{ cm}^{-1}$  seems to be somewhat more reasonable for  $\text{CrCl}_2$  than the one around  $495\text{ cm}^{-1}$ .

Kobra<sup>[8]</sup> and Hastie<sup>[7]</sup> measured several other bands that they assigned to dimeric or possibly trimeric species. Several of these agree with our computations, considering the evident uncertainties of both techniques. There is a wide and very intense peak in the high-temperature gas-phase spectrum<sup>[8]</sup> (about  $320\text{ cm}^{-1}$ ) that must include the monomer symmetric stretching frequency (we computed it between  $340\text{--}350\text{ cm}^{-1}$ ), but its IR intensity is rather small. There are, however, several medium intensity bands of the dimer and an intense band of the trimer in this region.

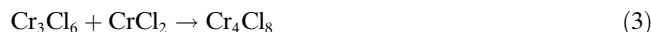
As we have  $[4(n-1)+2]$  Cr–Cl bonds for the  $(\text{CrCl}_2)_n$  clusters, we have  $4n-2$  Cr–Cl stretching frequencies in the  $\text{CrCl}_2$  chain. The two highest frequency modes are the symmetric and asymmetric terminal Cr–Cl<sub>i</sub> stretching modes. As expected, the coupling between the symmetric and asymmetric modes becomes smaller as the chain grows and the splitting between these two modes become smaller with only  $5\text{ cm}^{-1}$  left for the trimer. These frequencies branch out with growing cluster size, with the lowest stretching frequency starting from  $349\text{ cm}^{-1}$  for the monomer,  $265\text{ cm}^{-1}$  for the dimer, to  $213\text{ cm}^{-1}$  for the trimer; while the highest frequency decreases converging at around  $430\text{ cm}^{-1}$  with growing chain length at the B3LYP level of theory. The lowest frequencies for all of the clusters are the ring puckering, ring twisting, and terminal chlorine bending modes.

There are no experimental data reported for the bending frequency. This is the frequency for which the computations are the most vulnerable; they usually underestimate these modes by a considerable amount as the bending potential

can be quite shallow, see Figure 3. Our computations predict the bending mode for  $\text{CrCl}_2$  between  $25$  and  $57\text{ cm}^{-1}$ . For the first-row transition-metal dihalides from  $\text{MnCl}_2$  to  $\text{NiCl}_2$ , this frequency has been measured between about  $85\text{--}96\text{ cm}^{-1}$ . Based on this, our bending mode frequency of  $45\text{ cm}^{-1}$  as predicted by CCSD(T) is probably too small. Of course, the experimental bending frequencies could include considerable anharmonicity effects. However, our anharmonic analysis for the bending mode results in a decrease of this mode by only  $1\text{ cm}^{-1}$ , even less than the anharmonic contributions to the symmetric and asymmetric stretching frequencies that are about  $3\text{--}4\text{ cm}^{-1}$ .

The B3LYP and B3PW91 dipole moments for the global minima are  $2.267\text{ D}$  and  $2.430\text{ D}$  for the  $^3\text{B}_2$  state of the monomer, and  $1.082\text{ D}$  and  $1.728\text{ D}$  for the  $^1\text{A}_1$  state of the dimer **D1**, respectively. This compares to  $1.609\text{ D}$  (B3LYP) and  $2.119\text{ D}$  (B3PW91) for the  $^9\text{A}_1$  state of the dimer. Note that the *trans* structures contain inversion symmetry and yield no dipole moment.

**Thermodynamic analysis:** Vibrational analyses on the B3LYP global minima were carried out at  $298.15\text{ K}$  as well as from  $1000\text{--}2000\text{ K}$ . We calculated the values of  $\Delta H$  from statistical thermodynamics for the reactions given in Equations (1)–(3) to be  $-44.4$ ,  $-42.0$ , and  $-42.1\text{ kcal mol}^{-1}$ , respectively.



Based on the  $\Delta H_{298}^0$  values of sublimation for the monomer up to the tetramer from a mass spectrometric study by Ratkovskii et al.,<sup>[14]</sup> we calculated the values of  $\Delta H$  for the same reactions to be  $-55 \pm 4$ ,  $-53 \pm 5$ , and  $-56\text{ kcal mol}^{-1}$ , respectively, at standard conditions; the tetramer value is only an estimation. Ratkovskii and co-workers also determined the standard enthalpies of dissociation of the dimer, trimer, and tetramer to be  $55 \pm 4$ ,  $109 \pm 8$ , and  $156\text{ kcal mol}^{-1}$ , respectively. We obtained values of  $44.4$ ,  $86.4$ , and  $128.5\text{ kcal mol}^{-1}$ , respectively, for the same processes. Schoonmaker et al.<sup>[13]</sup> determined the  $\Delta H$  value of dissociation of the dimer at  $985\text{ K}$  to be  $47.9 \pm 3\text{ kcal mol}^{-1}$ . We obtained a value of  $42.7\text{ kcal mol}^{-1}$ . Hence our B3LYP  $\Delta H$  values for reactions given in Equations (1)–(3) are all too positive compared to the experimental values. Changing to B3PW91 or to any other hybrid or generalized gradient approximation does not improve this situation significantly.

Therefore we used the following approach: we calculated the dimerization energy by the CASPT2 method and used that as a basis to estimate all other dissociation energies. First, as each  $\text{CrCl}_2$  adds almost a constant value, we took the CASPT2 dimerization energy of  $54.0\text{ kcal mol}^{-1}$  and corrected it by the three- and four-body contributions from our B3LYP calculations. This gives changes in total electronic

energies (not including zero-point vibrational energy corrections) of  $\Delta E = -54.0 \text{ kcal mol}^{-1}$  for the reaction in Equation (1) as discussed above, and  $-51.7$  for reactions in Equations (2) and (3). Next, we took the thermodynamic analysis from our B3LYP calculation and added the finite temperature values to our CASPT2 energies. The corrected enthalpies,  $\Delta H$ , and free energies,  $\Delta G$ , at different temperatures are listed in Table 7. The reported  $\Delta H$  values are now in much better agreement with experiment, even though they might still be a bit low.

The reported thermodynamic properties should be useful for future gas-phase experiments. Unfortunately, we could not estimate the possible vapor composition at our ED experimental conditions. First of all, the vapor composition is very sensitive to slight changes in the  $\Delta G$  values. Moreover, the evaporation during the ED experiment is most likely a sublimation process, during which larger species might evaporate from the solid together with the monomeric molecules. The estimation of the thermodynamics of these processes is beyond our present possibilities.

## Conclusions

Chromium dichloride remains a challenging problem for both experimental and theoretical studies. From the computational point of view, handling an open electron-shell system requires special care. It has been shown previously<sup>[20,21]</sup> that ligand field theory is only a crude approximation for these systems, as there is a noticeable 3d–4s mixing, giving rise to low-lying, closely spaced electronic states. In this paper, complete active space calculations with different sizes of the active space were applied; together with multireference, second-order perturbation theory, and coupled cluster calculations, in order to treat both dynamic and nondynamic electron correlation for the monomer molecule. According to the literature, neither the electronic state nor the shape of the ground-state monomeric molecule have been known with certainty. Our extensive calculations determined that from among the possible electronic states of a linear molecule, the  $^5\Pi_g$  state has the lowest energy, but it is a saddle point, in agreement with the ramifications of the Renner–Teller effect.<sup>[56]</sup>

Chromium dichloride, with its  $d^4$  electronic configuration, is an interesting system in that it is subject to both the Jahn–Teller and the Renner–Teller effects; the former in its crystals and the latter in the gas phase. The chromium atom in

the crystal of  $\alpha\text{-CrCl}_2$  has a distorted (elongated) octahedral coordination according to both its X-ray diffraction<sup>[62]</sup> and computational<sup>[31]</sup> studies—a typical Jahn–Teller distortion of a high-symmetry octahedral coordination around a  $d^4$  metal.

According to the Renner–Teller effect, the lowest energy linear electronic state of the molecule,  $^5\Pi_g$ , splits into two nondegenerate states, of which the  $^5B_2$  state is the ground state from all but one of our calculations. Only the CASPT2 method puts the  $^5B_2$  electronic state above the  $^5\Sigma_g^+$  state by a mere 0.035 eV. The  $^5\Sigma_g^+$  state is about 0.16–0.28 eV higher in energy than the  $^5B_2$  state for all other computations. The other electronic states are much higher in energy and are not contestants for the electronic ground state.

Small clusters of  $\text{CrCl}_2$  from dimers to tetramers have been investigated. It was found that they all consist of antiferromagnetically coupled chains of  $\text{CrCl}_2$  molecules, forming four-membered rings, closely resembling the solid-state structure of  $\alpha\text{-CrCl}_2$ . The BS-DFT calculations might overestimate the stabilities of the coupled low-spin states.<sup>[67]</sup> The correlated ab initio methods predict that the high-spin states are the ground state, but this result is strongly method-dependent, and requires accurate multireference calculations. Nevertheless, the DFT calculations are in agreement with experimental results for the solid, in which the ground state is the antiferromagnetically coupled state.

From the possible structures for the dimer, the  $C_{2v}$  and  $C_{2h}$  symmetry structures are shown to have almost the same energy; therefore, both are candidates for the ground state for the dimer, with the  $C_{2v}$  structure being more stable than the pseudo Jahn–Teller distorted  $C_{2h}$  structure by less than 0.01 eV.

We re-analyzed the previously published ED data<sup>[3]</sup> taking into consideration the more complicated vapor composition than supposed in that study.<sup>[68]</sup> The major component of the vapor of chromium dichloride was the monomeric species. Beside that about 19(4)% dimers and 4(3)% trimers were also present, but their larger size means greater contributions to the molecular scattering (due to their larger number of atomic pairs) than their small percentage would indicate. We estimated the experimental equilibrium bond length of  $\text{CrCl}_2$  by anharmonic corrections,  $r_e^M(\text{Cr–Cl}) = 2.196(20) \text{ \AA}$ . This value, as well as the bond angle of the molecule, agrees very well with the computations. The unusually large uncertainties of the parameters are due to the complicated vapor composition and the very large correlations among the closely spaced distances belonging to the different species. The present ED analysis is in agreement with the previous

Table 7. Thermodynamic properties for the  $\text{CrCl}_2$  nucleation according to the reactions in Equations (1)–(3) in the text.

$T$ [K]	$\Delta H(1)$ [kcal mol <sup>-1</sup> ]	$\Delta G(1)$ [kcal mol <sup>-1</sup> ]	$\Delta S(1)$ [cal mol <sup>-1</sup> K <sup>-1</sup> ]	$\Delta H(2)$ [kcal mol <sup>-1</sup> ]	$\Delta G(2)$ [kcal mol <sup>-1</sup> ]	$\Delta S(2)$ [cal mol <sup>-1</sup> K <sup>-1</sup> ]	$\Delta H(3)$ [kcal mol <sup>-1</sup> ]	$\Delta G(3)$ [kcal mol <sup>-1</sup> ]	$\Delta S(3)$ [cal mol <sup>-1</sup> K <sup>-1</sup> ]
298.15	-51.8	-40.2	-39.0	-49.5	-37.9	-38.8	-49.6	-36.5	-43.7
1000	-50.1	-16.9	-33.2	-47.7	-12.6	-35.1	-47.8	-8.7	-39.0
1200	-49.3	-10.3	-32.5	-46.9	-5.6	-34.4	-47.0	-1.0	-38.3
1500	-48.1	-0.7	-31.6	-45.7	4.6	-33.5	-45.8	10.0	-37.2
2000	-46.1	14.8	-30.4	-43.7	21.7	-32.4	-43.8	28.8	-36.3

one in that the molecule is not linear; however, the bond angle from the present study is much larger than the one reported in reference [3]. The dibridged structure of the trimeric species, found to be the ground-state structure by our computations, is also in agreement with the experiment, while the usual structure of metal halide trimers, the six-membered ring structure, is not. The bridged structure of the dimeric and trimeric species can be considered as a first step in the nucleation process leading to the crystal of  $\text{CrCl}_2$ .

Young et al.<sup>[69]</sup> conclude their recent article on the shape of the  $\text{TiF}_2$  molecule with the following statement: "There is now no reliable experimental evidence for the nonlinearity of any first row transition-metal difluoride or dichloride." In view of our findings on the nonlinearity of  $\text{CrCl}_2$ , we offer the following comment. Our computations determined that this molecule undergoes Renner–Teller symmetry breaking, and within the adiabatic (Born–Oppenheimer) approximation—which strictly defines the structure of a molecule<sup>[70]</sup>—it is bent. It is comforting that the electron-diffraction experimental data are fully consistent with this finding. At this point it is of interest to look into the question: could the ED data alone be interpreted by a linear arrangement of the molecule? This question is not as straightforward as we might think, since ED yields a thermal average structure rather than the equilibrium structure, hence even a linear molecule appears to be bent in an ED analysis. Thus, the question is whether it might be possible to distinguish a bent thermal average structure from a genuinely nonlinear geometry? The shrinkage of the nonbonded  $\text{Cl}\cdots\text{Cl}$  distance for a linear metal dichloride molecule is always much larger than that of a truly bent molecule, so the thermal-average structure for such a linear molecule could be close to a truly bent one. There is a simple relationship between the bending frequency of a linear molecule and the shrinkage effect and, consequently, the bond angle of the molecule.<sup>[71]</sup> As we already discussed above, the computed bending frequencies of  $\text{CrCl}_2$  are much too small to be reliable. However, there are experimental frequencies available for several other transition-metal dichlorides.<sup>[2]</sup> In between  $\text{TiCl}_2$  ( $130\text{ cm}^{-1}$ ) and  $\text{CuCl}_2$  ( $122\text{ cm}^{-1}$ ), the bending frequencies of other first-row transition-metal dichlorides vary between about  $85\text{--}95\text{ cm}^{-1}$ . Thus, it seems reasonable to suppose that the gas-phase bending frequency of  $\text{CrCl}_2$  would not be smaller than, say,  $90\text{--}100\text{ cm}^{-1}$ . We performed structure analyses with bond angles constrained at values corresponding to bending frequencies in the region between  $60\text{--}120\text{ cm}^{-1}$ . The agreement with experiment somewhat worsened compared with the structure with the refined  $149^\circ$  bond angle. However, whenever the constraint on the bond angle was lifted, it always refined to the  $149^\circ$  value. We also checked which bending frequency would correspond to a thermal average bond angle of  $149^\circ$  for a molecule for which the equilibrium structure would be linear. The corresponding  $\nu_3$  was  $73\text{ cm}^{-1}$ . This value appears far too low considering the trend of the bending frequency variation among the first row transition-

metal dichlorides. This observation lends additional support for the nonlinearity of  $\text{CrCl}_2$ .

## Acknowledgements

The Auckland group acknowledges financial support through a Marsden grant administered by the Royal Society of New Zealand. B.V. and A.H. would like to thank Education New Zealand and Massey University for financial support. The Budapest group acknowledges the financial support of the Hungarian Scientific Research Fund (Grant No. OTKA K 60365).

- [1] M. Hargittai, *Coord. Chem. Rev.* **1988**, *91*, 35.
- [2] M. Hargittai, *Chem. Rev.* **2000**, *100*, 2233.
- [3] M. Hargittai, O. V. Dorofeeva, J. Tremmel, *Inorg. Chem.* **1985**, *24*, 3963.
- [4] E. Z. Zazorin, A. G. Gershiokov, V. P. Spiridonov, A. A. Ivanov, *Zh. Strukt. Khim.* **1987**, *28*, 56.
- [5] M. E. Jacox, D. E. Milligan, *J. Chem. Phys.* **1969**, *51*, 4143.
- [6] J. W. Hastie, R. Hauge, J. L. Margrave, *J. Chem. Soc. D* **1969**, 1452.
- [7] J. W. Hastie, R. Hauge, J. L. Margrave, *High Temp. Sci.* **1971**, *3*, 257.
- [8] V. M. Kovba, *Zh. Neorg. Khim.* **1983**, *28*, 2689.
- [9] J. S. Ogden, R. S. Wyatt, *J. Chem. Soc. Dalton Trans.* **1987**, 859.
- [10] R. J. M. Konings, A. S. Booi, *J. Mol. Struct.* **1992**, *269*, 39.
- [11] P. D. Gregory, J. S. Ogden, *J. Chem. Soc. Dalton Trans.* **1995**, 1423.
- [12] R. J. M. Konings, *High Temp. Mater. Sci.* **1996**, *35*, 105.
- [13] R. C. Schoonmaker, A. H. Friedman, R. F. Porter, *J. Chem. Phys.* **1959**, *31*, 1586.
- [14] P. A. Ratkovskii, T. A. Pribitkova, P. V. Galickii, *Teplofiz. Vys. Temp.* **1974**, *12*, 731.
- [15] I. R. Beattie, *Angew. Chem.* **1999**, *111*, 3494; *Angew. Chem. Int. Ed.* **1999**, *38*, 3294.
- [16] C. W. DeKock, D. M. Gruen, *J. Chem. Phys.* **1966**, *44*, 4387.
- [17] C. W. DeKock, D. M. Gruen, *J. Chem. Phys.* **1968**, *49*, 4521.
- [18] C. D. Garner, I. H. Hillier, C. Wood, *Inorg. Chem.* **1978**, *17*, 168.
- [19] S. Smith, I. H. Hillier, *J. Chem. Soc. Commun.* **1989**, 539.
- [20] S. G. Wang, W. H. E. Schwarz, *J. Chem. Phys.* **1998**, *109*, 7252.
- [21] A. J. Bridgeman, C. H. Bridgeman, *Chem. Phys. Lett.* **1997**, *272*, 173.
- [22] V. R. Jensen, *Mol. Phys.* **1997**, *91*, 131.
- [23] I. M. B. Nielsen, M. D. Allendorf, *J. Phys. Chem. A* **2005**, *109*, 928.
- [24] N. Schiefenhövel, M. Binnewies, F. Janetzko, K. Jug, *Z. Anorg. Allg. Chem.* **2001**, *627*, 1513.
- [25] X. Li, J. Paldus, *J. Chem. Phys.* **2007**, *126*, 234303.
- [26] Y. Zhao, D. G. Truhlar, *J. Chem. Phys.* **2006**, *124*, 224105.
- [27] A. Görling, S. B. Trickey, P. Gisdakis, N. Rösch, *Top. Organomet. Chem.* **1999**, *4*, 109.
- [28] M. Cococcioni, S. de Gironcoli, *Phys. Rev. B* **2005**, *71*, 035105.
- [29] V. I. Anisimov, J. Zaanen, *Phys. Rev. B* **1991**, *44*, 943.
- [30] J. N. Harvey, *Struct. Bonding* **2004**, *112*, 151.
- [31] A. Hermann, B. Vest, P. Schwerdtfeger, *Phys. Rev. B* **2006**, *74*, 224402.
- [32] J. P. Perdew, J. A. Chevary, S. H. Vosko, K. A. Jackson, M. R. Pederson, D. J. Singh, C. Fiolhais, *Phys. Rev. B* **1992**, *46*, 6671.
- [33] T. H. Dunning, P. J. Hay, *Methods of Electronic Structure, Theory*, Vol. 2, Plenum, New York, **1977**.
- [34] P. J. Hay, W. R. Wadt, *J. Chem. Phys.* **1985**, *82*, 270.
- [35] A. D. Becke, *J. Chem. Phys.* **1993**, *98*, 5648.
- [36] C. Lee, W. Yang, R. G. Parr, *Phys. Rev. B* **1988**, *37*, 785.
- [37] S. H. Vosko, L. Wilk, M. Nusair, *Can. J. Phys.* **1980**, *58*, 1200.
- [38] P. J. Stephens, F. J. Devlin, C. F. Chabalowski, M. J. Frisch, *J. Phys. Chem.* **1994**, *98*, 11623.
- [39] M. Dolg, U. Wedig, H. Stoll, H. Preuss, *J. Chem. Phys.* **1987**, *86*, 866.
- [40] D. E. Woon, T. H. Dunning, *J. Chem. Phys.* **1993**, *98*, 1358.
- [41] Gaussian 03 (Revision C.03), M. J. Frisch, G. W. Trucks, H. B. Schlegel, G. E. Scuseria, M. A. Robb, J. R. Cheeseman, J. A. Montgomery, Jr., T. Vreven, K. N. Kudin, J. C. Burant, J. M. Millam, S. S. Iyengar,

- gar, J. Tomasi, V. Barone, B. Mennucci, M. Cossi, G. Scalmani, N. Rega, G. A. Petersson, H. Nakatsuji, M. Hada, M. Ehara, K. Toyota, R. Fukuda, J. Hasegawa, M. Ishida, T. Nakajima, Y. Honda, O. Kitao, H. Nakai, M. Klene, X. Li, J. E. Knox, H. P. Hratchian, J. B. Cross, V. Bakken, C. Adamo, J. Jaramillo, R. Gomperts, R. E. Stratmann, O. Yazyev, A. J. Austin, R. Cammi, C. Pomelli, J. W. Ochterski, P. Y. Ayala, K. Morokuma, G. A. Voth, P. Salvador, J. J. Dannenberg, V. G. Zakrzewski, S. Dapprich, A. D. Daniels, M. C. Strain, O. Farkas, D. K. Malick, A. D. Rabuck, K. Raghavachari, J. B. Foresman, J. V. Ortiz, Q. Cui, A. G. Baboul, S. Clifford, J. Cioslowski, B. B. Stefanov, G. Liu, A. Liashenko, P. Piskorz, I. Komaromi, R. L. Martin, D. J. Fox, T. Keith, M. A. Al-Laham, C. Y. Peng, A. Nanayakkara, M. Challacombe, P. M. W. Gill, B. Johnson, W. Chen, M. W. Wong, C. Gonzalez, and J. A. Pople, Gaussian, Inc., Wallingford, CT, **2004**.
- [42] B. Réffy, C. J. Marsden, M. Hargittai, *J. Phys. Chem. A* **2003**, *107*, 1840.
- [43] M. Hargittai, B. Réffy, M. Kolonits, *J. Phys. Chem. A* **2006**, *110*, 3770.
- [44] Z. Neizer, Z. Varga, G. Jancsó, M. Hargittai, *Struct. Chem.* **2007**, *18*, 641.
- [45] H.-J. Werner, P. J. Knowles, R. Lindh, F. R. Manby, M. Schütz, P. Celani, T. Korona, G. Rauhut, R. D. Amos, A. Bernhardsson, A. Berning, D. L. Cooper, M. J. O. Deegan, A. J. Dobbyn, F. Eckert, C. Hampel, G. Hetzer, A. W. Lloyd, S. J. McNicholas, W. Meyer, M. E. Mura, A. Nicklass, P. Palmieri, R. Pitzer, U. Schumann, H. Stoll, A. J. Stone, R. Tarroni, T. Thorsteinsson, Molpro, version 2006.1, a package of ab initio programs, **2006**. see <http://www.molpro.net>.
- [46] S. F. Boys, F. Bernardi, *Mol. Phys.* **1970**, *19*, 533.
- [47] F. B. van Duijneveldt, J. G. C. M. van Duijneveldt-van de Rijdt, J. H. van Lenthe, *Chem. Rev.* **1994**, *94*, 1873.
- [48] P. E. Blöchl, *Phys. Rev. B* **1994**, *50*, 17953.
- [49] G. Kresse, D. Joubert, *Phys. Rev. B* **1999**, *59*, 1758.
- [50] G. Kresse, J. Furthmüller, *Phys. Rev. B* **1996**, *54*, 11 169.
- [51] A. W. Ross, M. Fink, R. Hilderbrandt, J. Wang, V. H. Smith, Jr., *International Tables for Crystallography C*, Kluwer, Dordrecht, **1995**, p. 245.
- [52] M. Hargittai, I. Hargittai, *Int. J. Quantum Chem.* **1992**, *44*, 1057.
- [53] M. Hargittai, N. Y. Subbotina, M. Kolonits, A. G. Gershikov, *J. Chem. Phys.* **1991**, *94*, 7278.
- [54] L. Hedberg, I. M. Mills, *J. Mol. Spectrosc.* **1993**, *160*, 117.
- [55] B. O. Roos, K. Andersson, M. P. Fülscher, P. Malmqvist, L. Serrano-Andrés, K. Pierloot, M. Merchán, *Advances in Chemical Physics, Vol. XCIII*, Wiley, New York, **1996**, p. 219.
- [56] R. Renner, *Z. Phys.* **1934**, *92*, 172.
- [57] I. B. Bersuker, *Chem. Rev.* **2001**, *101*, 1067.
- [58] L. v. Szentpály, P. Schwerdtfeger, *Chem. Phys. Lett.* **1990**, *170*, 555.
- [59] L. Wharton, R. A. Berg, W. Klemperer, *J. Chem. Phys.* **1963**, *39*, 2023.
- [60] F. Grein, *Chem. Phys. Lett.* **2008**, *455*, 124.
- [61] H. R. Oswald, *Helv. Chim. Acta* **1961**, *44*, 1049.
- [62] J. W. Tracy, N. W. Gregory, E. C. Lingafelter, J. D. Dunitz, H.-C. Mez, R. E. Rundle, C. Scherlinger, H. L. Yakel Jnr, and M. K. Wilkinson, *Acta Crystallogr.* **1961**, *14*, 927.
- [63] M. Hargittai, P. Schwerdtfeger, B. Réffy, R. Brown, *Chem. Eur. J.* **2003**, *9*, 327.
- [64] M. Hagiwara, K. Katsumata, *J. Magn. Magn. Mater.* **1995**, *140*, 1665.
- [65] M. Winkelmann, M. Baehr, M. Reehuis, M. Steiner, M. Hagiwara, K. Katsumata, *J. Phys. Chem. Solids* **1997**, *58*, 481.
- [66] I. R. Rudra, Q. Wu, T. V. Voorhis, *J. Chem. Phys.* **2006**, *124*, 9.
- [67] Y. Zhao, D. G. Truhlar, *Acc. Chem. Res.* **2008**, *41*, 157.
- [68] In that early study, we referred to a recent, yet unpublished study of CrCl<sub>2</sub> according to which the molecule was linear. Many later publications on the structure of CrCl<sub>2</sub> quoted that unpublished study in order to lend support to the notion that there exists a contradiction between the two ED results. After many years, the unpublished study remains inaccessible, and we must suppose that its findings are suspect and suggest that they be ignored in further discussions.
- [69] A. V. Wilson, A. J. Roberts, N. A. Young, *Angew. Chem.* **2008**, *120*, 1798; *Angew. Chem. Int. Ed.* **2008**, *47*, 1774.
- [70] H. Primas, U. Müller-Herold, *Elementare Quantenchemie*, Teubner, Stuttgart, **1990**.
- [71] S. J. Cyvin, *Molecular Vibrations and Mean Square Amplitudes*, Elsevier, Amsterdam, **1968**.

Received: February 22, 2008

Published online: May 19, 2008